JOURNAL OF OPTOELECTRONICS AND ADVANCED MATERIALS, Vol. 11, No. 12, December 2009, p. 1899 - 1906

Effect of photo-oxidation on the photodiffusion of silver in germanium chalcogenide glasses

M. MITKOVA[a*], A. KOVALSKIY[b], H. JAIN[b] Y. SAKAGUCHI[a,c]
[a]*Department of Electrical and Computer Engineering, Boise State University, 1910 University Dr., Boise, ID 83725-2075, USA*
[b]*Department of Materials Science, Lehigh University, 5 East Packer Avenue, Bethlehem, PA 18015-3195, USA*
[c]*Now with Japan Atomic Energy Agency (JAEA), 2-4 Shirane, Shirakata, Tokai-mura Naka-gun, Ibaraki 319-1195, Japan*

We report results on photoinduced changes in Ge-chalcogenide glasses, which occur in ultra high vacuum (UHV) vs. in air. They demonstrate the important role of oxygen that determines the magnitude and the type of the photoinduced effects. To observe photodiffusion without the presence of oxygen, Ag/glass thin films were prepared, subjected to photodiffusion, and chemically analyzed, all within the chamber of high resolution X-ray Photoelectron Spectroscopy (XPS) equipment. Under these oxygen-free conditions, Ag is introduced in the Ge-Se hosting network. The results show that the diffusion product is homogeneous, comprising of Ge-chalcogen tetrahedra and ethane-like units $(GeSe_3)_2$ with Ag^+ ions attached to them. In oxygen containing ambient, Ge rich glasses oxidize more easily than the chalcogen rich glasses, since oxygen reacts primarily with Ge. Under these experimental conditions, which are likely to exist in practical applications, a higher concentration of Ag can be introduced, with the formation of Ag containing products like α and β Ag_2Se and Ag_8GeSe_6. Raman spectroscopy reveals that because of interaction between Ge and oxygen, the initially Ge-rich chalcogenide network becomes chalcogen-rich after the oxidation of Ge.

(Received July 5, 2009; accepted November 12, 2009)

Keywords: Chalcogenide glasses, Ag photodiffusion, oxidation, Raman spectroscopy, X-ray photoelectron spetroscopy

1. Introduction

Photo-induced effects are among the most explored properties of chalcogenide glasses (ChG), which lead to number of applications [1,2]. These effects arise from the changes that occur from their interaction with light [3]. In simple terms, a given effect results from the changes in physical (atom positions, degree of disorder, etc.), chemical (composition, bonding among the atoms, etc.), electronic (density of states in the valence and conduction bands) and/or vibrational (modes of vibrations of structural units) structures [4-6].

For a long time it was believed that the observed effects arise solely from the interaction of chalcogenide matrix with light, although the experiments were performed in the ambient, i.e. without any precautions to avoid oxidation. However, works of Chopra [7], Ke. Tanaka [8], Spence and Elliott [9], etc. demonstrated significant influence of oxygen on the photoinduced effects, in particular their dependence on irradiation dose. Tichy et al. [10,11] reported three bands in the infrared (IR) spectra of Ge-S glasses at 870, 820, and 800 cm^{-1} occurring after interaction with light in ambient atmosphere. The first band was assigned to the dominant mode of GeO_2 structure, whereas the other features were related to the Ge-O stretching within S_{3-x}-O_x-Ge-O-Ge-O_xS_{3-x} clusters. With increasing amount of oxygen in the structure, a shift occurred towards smaller wave numbers because of higher local electronegativity. Notwithstanding, the effect of photo-oxidation on properties has remained poorly characterized.

Photoinduced oxidation has been controversial because it is difficult to characterize it in a short term experiment related to photoinduced effects. Often there is also ambiguity regarding the identity of the oxide, whether that of the chalcogen or the remaining elements, usually from the 4^{th} or 5^{th} group of the periodic table. For example, there are reports of the formation of oxides of Ge [10,11], yet Harshavardhan et. al. [7,12] have reported weight and thickness losses in obliquely deposited films presumably from the formation of volatile chalcogen oxides. The lack of these effects in normally deposited films and the difference in the behaviour of S and Se containing films have been, however, very vaguely explained. For example, one may understand the evaporation of oxides as responsible for photo-contraction, but this cannot explain photoexpansion, occurring in some cases. One interpretation of the observed effect of film thickness reduction from photo-oxidation suggests that the oxide film located on the surface produces strain at the interface, and thus creates states into the energy band gap. This explanation is inconsistent with a general view that oxidation leads to the bleaching of thin chalcogenide glass films [13].

To resolve some of the above mentioned conflicting observations and their explanations, we have compared photoinduced effects realized in vacuum and in air within Ge-chalcogenide glass films. The results are obtained with respect to the initial glass composition and products

accompanying Ag photodiffusion. The structure and composition of the films are characterized by high resolution X-ray photoelectron spectroscopy (XPS) and Raman spectroscopy. We focus on visible light as well as X-ray induced diffusion, since as reported earlier [14,15] and also established by us [16] not only band gap light but also X-ray photons cause Ag - photodiffusion.

2. Experimental

The experiments were performed on thin films deposited using thermal vacuum evaporation. Selenium containing films were prepared from bulk Ge_{30} Se_{70} and $Ge_{40}Se_{60}$ glasses on HF-etched Si wafers (Wacker Siltronic Corp., 525 ± 20 μm thickness); silver thin films were deposited on top of the chalcogenide films. The films forming the sandwich were deposited in an Edwards E306A vacuum coating system, and then handled in air. The thickness of the films was 200 nm for nominal composition $Ge_{30}Se_{70}$, and 400 nm for the $Ge_{40}Se_{60}$ nominal composition; Ag films were 11.5 nm thick.

$Ge_{30}Se_{70}$ films were also prepared inside the ultra-high vacuum of XPS spectrometer so that film formation, radiation and characterization were performed without exposing them to atmosphere. The thickness of such films was not controllable but it was more than ~12 nm (estimated depth of analysis for ESCA-300 XPS spectrometer) since the signal from Si substrate was not detectible by XPS measurements. From the time of deposition, we estimate the thickness of the film at ~ 50 nm. A 12 nm thick silver layer was deposited in 3 steps (1 nm, 2 nm and 9 nm) on top of $Ge_{30}Se_{70}$ film under the same conditions. XPS measurements were performed after each of these silver deposition steps.

The Ge-S films were prepared by thermal evaporation on a silicon substrate in a Cresington 308R Desktop Coating System from previously synthesised glasses with composition $Ge_{40}S_{60}$. This method of films formation results in a relaxed films which makes it possible to compare the film's structure to that of bulk materials with the same composition. The thickness of the films was 300 nm. The composition of the as-prepared films was determined with an electron probe micro-analyzer in the scanning electron microscope system (LEO 1430VP) using energy dispersive x-ray spectroscopy (EDS) analysis which established that the films composition is $Ge_{46}S_{54}$. Raman spectra were recorded in backscattering geometry at room temperature using a Jobin Yvon T64000 triple spectrometer equipped with a liquid-nitrogen-cooled multichannel coupled-charge-device detector. The spectra were recorded at every minute to follow the evolution of the spectra in time under continuous laser radiation. The 441.6 nm laser line of the helium-cadmium continuous wave laser (Kimmon Koha Co., Ltd. IK5752 I-G) with the power of ~80 mW at the sample surface was used for the excitation and long term illumination.

Films were irradiated either with light of a halogen lamp emitting in the region 420-440 nm at 85 mW/cm^2 (RX Firefly, Phoseon Technology), with helium-cadmium continuous wave laser emitting at 441.6 nm, 85 mW; or with x-rays in the XPS system.

The XPS spectra (core levels and valence band) were recorded on a Scienta ESCA-300 spectrometer that uses monochromatic Al K_α X-rays (1486.6 eV) for excitation. The instrument was operated in a mode that yielded a Fermi-level width of 0.4 eV for Ag metal and a full width at half maximum (FWHM) of 0.54 eV for Ag $3d_{5/2}$ core level peak. Energy scale was calibrated using the Fermi level of clean Ag. The surface charging from photoelectron emission was controlled by flooding the surface with low energy (< 10 eV) electrons. The raw data were calibrated according to the gold $4f_{7/2}$ (84.0 eV) peak position. Data analysis was conducted with standard CASA-XPS software package. For analyzing the core-level spectra, Shirley background was subtracted and a Voigt line-shape, which results from a superposition of independent Lorentzian and Gaussian line broadening mechanisms, was assumed for the peaks [16]. Each 3*d* core-level spectrum for Ge and Se in our samples consisted of one or more spin orbit doublets splitting into $d_{5/2}$ and $d_{3/2}$ components. Fitting of Ag $3d_{5/2}$ spectra was carried out with single components only. The experimental error in the peak position and area of each component was ±0.05 eV and ±2 %, respectively. More detailed description of fitting procedure can be found elsewhere [17].

In the case of photodiffusion, the thermodynamics of the reaction is such that the diffusion reaction products at saturation can be nanocrystalline and, therefore, they were characterized also using X-Ray Diffraction (XRD) [18]. The particular conditions in our study were as follows: the XRD was carried out under 1° glancing angle with CuK_α emission λ=0.15418 nm and a 2θ range from 10° to 60° with 0.002 degree step width and 1 sec/degree time per step. Total scanning time was 7 hrs. The crystalline phases of the diffusion products in the films were identified from the XRD analysis, and the cluster sizes were calculated using Scherrer equation (1):

$$t = 0.9\lambda/B\cos\theta_B \quad (1)$$

where t is the size of the crystallites (in angstroms), λ the X-ray wavelength and θ_B the Bragg angle. The line broadening, B, is measured from the peak width at half the peak height in radians. The particle size was obtained by averaging the data over each peak of a particular composition.

3. Results

3.1 Short term photo-oxidation of Ge–Se glasses in air

The 200 nm thick $Ge_{30}Se_{70}$ films were irradiated with visible light for 15 minutes in air and XPS spectra were collected subsequently. Both Ge 3d and Se 3d core level spectra show 2 doublets from curve fitting (Fig. 1). The major peaks at 30.8 eV (Ge $3d_{5/2}$) and 54.3 eV (Se $3d_{5/2}$)

correspond to tetrahedral $GeSe_4$ and Ge-Se-Ge fragments, respectively [16]. Minor components at 30.2 eV and 54.8 eV relate to structural fragments with "wrong" homopolar Ge-Ge and Se-Se bonds. The concentration of homopolar Ge-Ge bonds is very small in this Ge-poor film (~4 % of all Ge atoms according to the relative areas of XPS peaks). The concentration of Se-Se bonds is much higher (~12 % of all Se atoms) as expected from the chemical composition. There are no oxygen related structural units represented in the fits, which means that at these conditions no oxidation products are observed within the resolution of the method. So we infer that Se rich compositions do not oxidize when exposed to limited visible light in air.

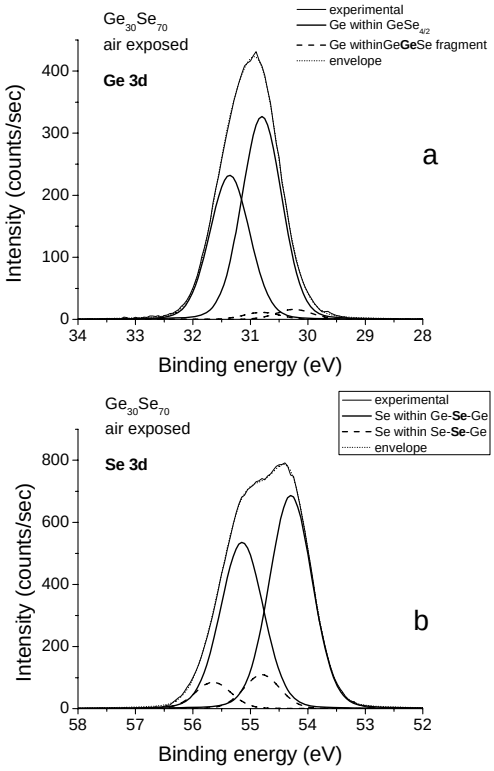

Fig. 1. XPS Ge 3d (A) and Se 3d (b) core level spectra of $Ge_{30}Se_{70}$ thin film exposed to air.

The XPS spectra for $Ge_{40}Se_{60}$ films, processed as the $Ge_{30}Se_{70}$ films above, are shown in Fig. 2. These glasses mostly consist of ethane like structural units $(Ge_2Se_{1/2})_6$ [19]. The Ge 3*d* core level spectrum (Fig. 2a) also contains two minor components but at higher binding energies, which we assign to the presence of oxidation. The Se 3d peak (Figure 2b) consists of only one doublet associated with 2-fold coordinated Se in the Se-poor structure.

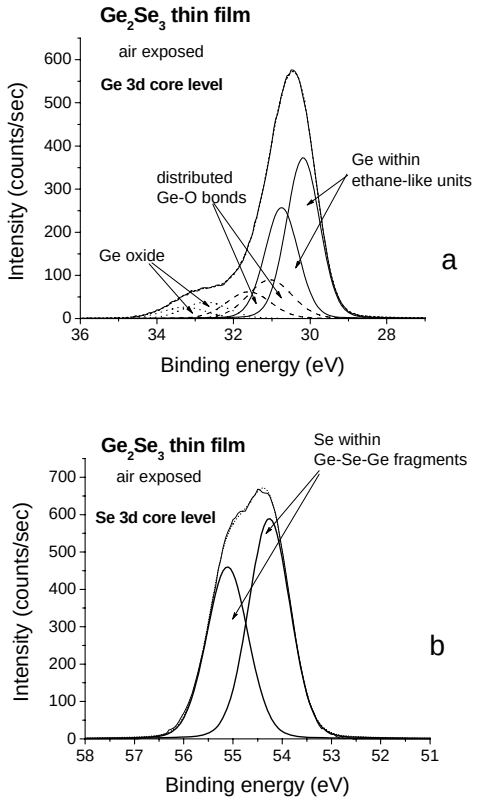

Fig. 2. XPS Ge 3d (a) and Se 3d (b) core level spectra of $Ge_{40}Se_{60}$ thin film exposed to air

3.2 Long term photo-oxidation of $Ge_{46}S_{54}$ glasses

Fig. 3 shows the structural evolution as depicted by Raman spectroscopy of films that were continuously illuminated with the laser beam. The top spectrum was measured in the first minute. It is comparable to that of $Ge_{40}S_{60}$ bulk, $Ge_{45}S_{55}$ bulk and $Ge_{40}S_{60}$ film, measured by other researchers [20, 21]. In the initial short period from 8 to 10 minutes of laser radiation, the material obviously undergoes structural changes, which are evident from the evolution of the Raman spectrum. After 21 minutes of irradiation, the peaks at 250 and 350 cm^{-1} become well pronounced and the spectrum remains stable. We have also found compositional changes in the films after long term illumination. The EDS spectra recorded at the illumination spot, showed a distinct presence of oxygen (about 17.7 at %), as shown in figure 4 compared to the initial composition of the film. The development of the oxidation process with time is shown on Figure 5. It is obvious that after 30 minutes of illumination this process starts to saturate.

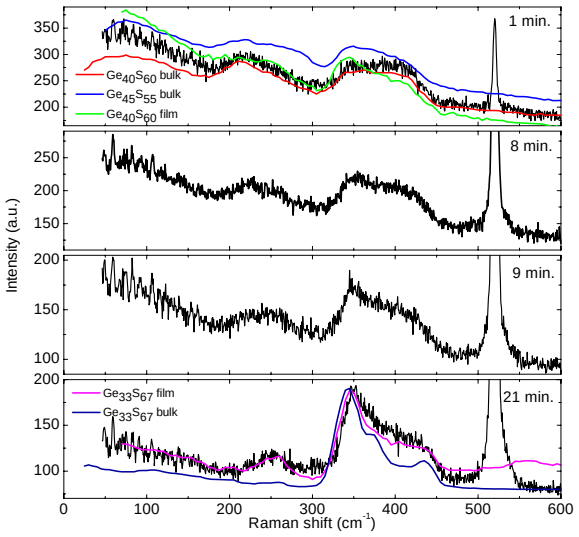

Fig. 3. Time evolution of Raman spectrum of Ge-S film, measured in air (solid black curves). Each spectrum was obtained by the average of 5 spectra with the accumulation time of 10 sec. The coloured solid curves are the spectra measured by Kotsalas and Raptis [21].

The illuminated area can be easily recognised as its color changes from light red to blue, as shown on figure 6 by the optical microscope images recorded after different times of irradiation.

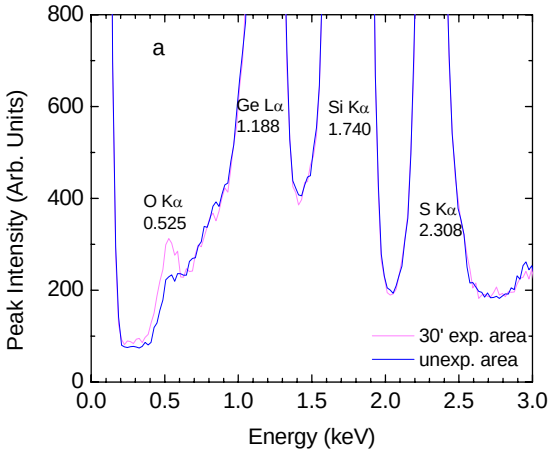

Fig. 4. EDS data for the composition of a $Ge_{46}S_{54}$ glass composition after 30" laser illumination. Note that the initial composition before the illumination is given for comparison.

3.3 Photodiffusion of Ag in vacuum

To compare the photodiffusion products forming from exposure in air with those forming in the absence of oxygen, we prepared the films inside the XPS chamber, irradiated them and then characterized, all within the at UHV conditions of spectrometer so that all the fabrication and characterization steps were conducted without any exposure to air. Both Ge 3*d* and Se 3*d* core level spectra of the surface of freshly deposited $Ge_{30}Se_{70}$ thin film exhibit two doublet components (at 30.8 eV and 30.2 eV for Ge $3d_{5/2}$; 54.3 eV and 54.8 eV for Se $3d_{5/2}$). The Ge/Se ratio of the deposited film matches well with that of the bulk glass used for evaporation, resulting in $Ge_{30}Se_{70}$ films.

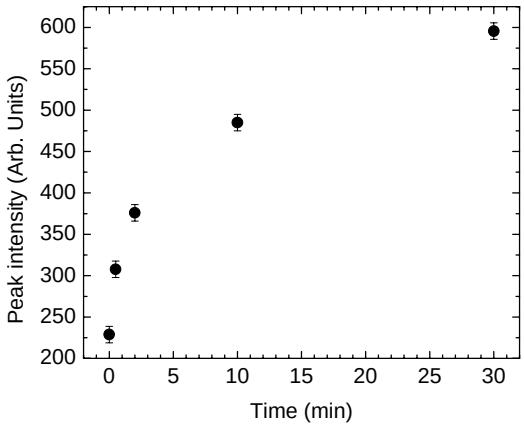

Fig. 5. Oxygen peak intensity as a function of irradiation time.

Next, silver was deposited on top of the $Ge_{30}Se_{70}$ film in three steps. X-rays served simultaneously as probe beam and irradiation causing silver diffusion. The ultimate chemical composition of the surface layer upon photodiffusion depends on the thickness of Ag layer. The maximum content of Ag in the matrix is close to 30 at.%. Binding energy for both Ge 3d and Se 3d core level spectra shifts gradually to lower values with increasing thickness of Ag layer (figure 7). This considerable change is a consequence of structural rearrangement with the disappearance of $GeSe_4$ tetrahedral units that are supposed to be the main constituents of a Se rich $Ge_{30}Se_{70}$ thin film. Instead of $GeSe_4$, the ternary composition, forming after the diffusion of Ag, shows appearance of some Ge–Ge bonds. The presence of such bonds is indicated by the estimated chemical shift from the change in the chemical environment and/or oxidation number of Ge atoms, with respect to that of Ge in $GeSe_4$ tetrahedron. In fact, at saturation (~30 at. % Ag) ethane-like $(GeSe_3)_2$ units are formed separately in the matrix by the diffused silver ions [16].

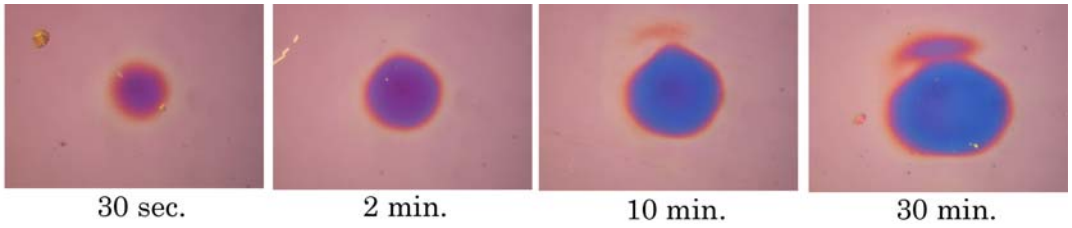

Fig. 6. Microscope images of the laser illuminated spot.

A recent XPS analysis showed [16] that after photoinduced diffusion, silver is in ionic state, distinct from the metallic Ag. The evolution of Ag diffusion into the film is clearly seen when comparing the valence band spectra of the samples just after Ag deposition and in equilibrium state (figure 8). For clarity, intermediate spectra are omitted on the figure. The structure of Ag 4d peak at binding energy (BE) of 5.5 eV is more complex at the beginning of Ag diffusion, revealing a distinct additional component at the low-BE side. The peak narrows in the equilibrium state supporting stable phase formation as the photodiffusion process is accomplished.

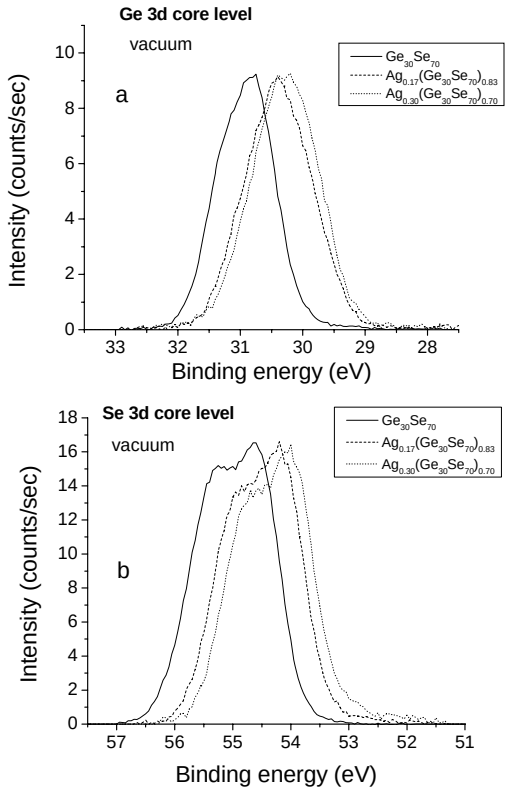

Fig. 7. Chemical shift of XPS Ge 3d and Se 3d core level spectra due to Ag photodiffusion into $Ge_{30}Se_{70}$ thin film prepared at UHV conditions.

3.4 Photodiffusion of Ag in air

Deposition of 11.5 nm thick Ag layer on top of $Ge_{30}Se_{70}$ thin films prepared in a separate vacuum deposition system and then exposed to air before the XPS measurements also shows a shift of Ge 3d and Se 3d core level peak positions towards the lower binding energies (figure 9). Because the $Ge_{30}Se_{70}$ thin film is much thicker in this case (200 nm in comparison with the estimated ~ 50 nm for UHV prepared sample), we are not able to reach saturation of Ag dissolution after depositing the 11.5 nm Ag layer. That is why the concentration of Ag at the surface in equilibrium after irradiation with 15 mW/cm^2 halogen lamp is only 15.6 at% instead of ~30 at%. This stage of photodiffusion may be compared with the intermediate, non-equilibrium stage for the sample prepared in UHV and discussed in the previous section. Note, however, that there is significant difference in Ag $3d_{5/2}$ position – almost 1 eV between the two samples. It suggests that Ag in the sample exposed to air is not in ionic but mostly in covalently bonded state within Ag-containing phase.

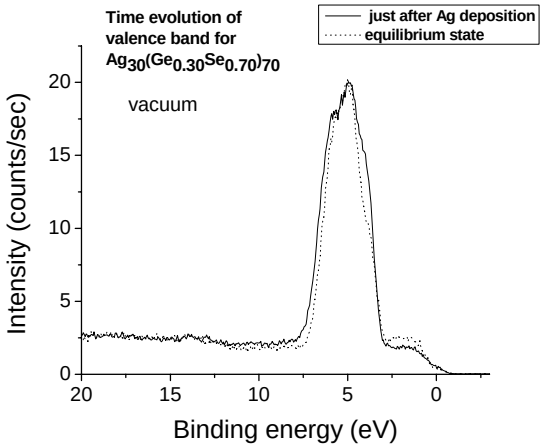

Fig. 8. Evolution of XPS valence band spectrum of $Ag/Ge_{30}Se_{70}$ sandwich deposited at UHV conditions and irradiated by X-rays of XPS spectrometer.

When photodiffusion is established in oxygen containing environment, the diffusion products are much more complex. Figure 10 shows XRD spectrum of an Ag photodiffused glass with initial composition $Ge_{30}Se_{70}$. In all instances, the hosting Ge-Se glass remains amorphous during illumination, while the silver containing species form nanocrystals. From diffraction peaks the composition and size of nanocrystals are estimated as follows: orthorhombic Ag_2Se with peaks at 2θ = 33.510, 34.882 (JCPDS card 20-1063; 39.083, 41.378, 42.365, and 25-

0766); cubic Ag_2Se with 2θ=35.891 (JCPDS card 27-0619), and Ag_8GeSe_6 with 2θ 27.139, 28.070, 46.976 and 49.357 (JCPDS card 71-1690). The size of the Ag containing crystals is estimated to be between 4 and 6 nm.

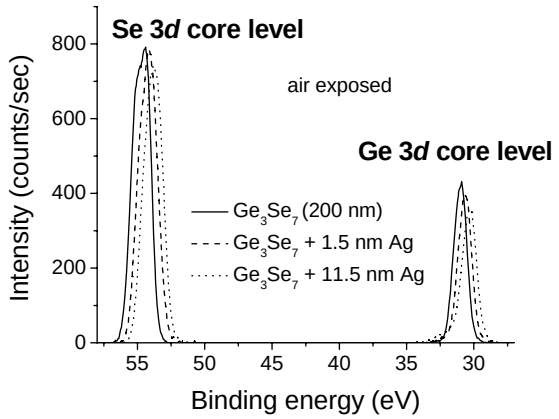

Fig. 9. Chemical shift of XPS Ge 3d and Se 3d core level spectra due to Ag photodiffusion into $Ge_{30}Se_{70}$ thin film under irradiation in air by halogen lamp (15 mW/cm^2).

Curve fitting of Ge 3d core level XPS peak after silver dissolution reveals some oxidation of germanium with the formation of two different oxides (figure 11) and approximately 9% of all Ge atoms are oxidized. There is no evidence for the formation of Se-O bonds in solid state.

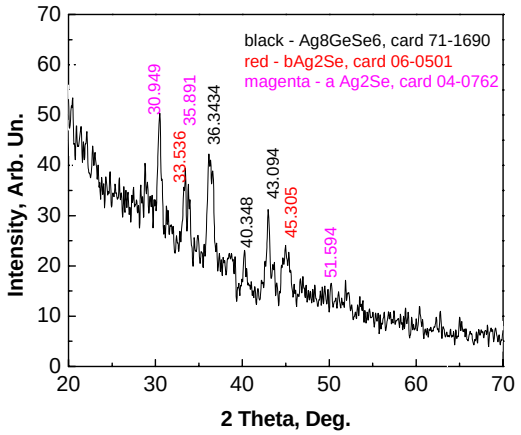

Fig. 10. XRD compositional data for a Ag doped in a presence of oxygen $Ge_{30}Se_{70}$ film.

4. Discussion

First let us discuss the dependence of oxidation kinetics on the composition of chalcogenide glass. The XPS spectra in figs. 1 and 2 show evidences that (i) oxidation process is related mainly to Ge atoms, and (ii) Se rich glasses do not oxidize to a detectable level. According to the standard potential data for the formation of bivalent oxides

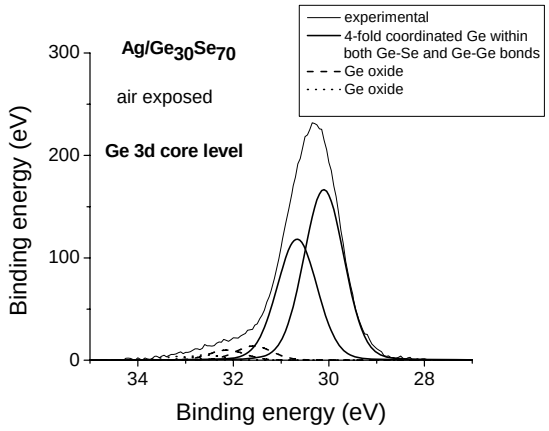

Fig. 11. XPS Ge 3d core level spectrum of Ag/$Ge_{30}Se_{70}$ thin film system irradiated in air by halogen lamp (15 mW/cm^2)

E^0/E^{n-2} [22], Ge is more easily oxidizable with potential V_{Ge} = 0.23 than S or Se with oxidation potential 0.54 and 0.74, respectively. Consequently, upon exposure to light illumination and formation of defects on Ge and Se sites, Ge is oxidized first. In the case of Se rich glasses, the structure of the material is built up by corner sharing and edge sharing units in which the bond energy of the Ge-Se bonds is 271 kJ/mol. A significant proportion of paired edge-sharing tetrahedra changes to corner sharing structure due to preferential breaking of the corresponding fourfold coordinated Ge containing structural units. However the general heterogeneous covalent Ge-Se bonding remains unchanged and so oxidation does not occur easily.

In the case of Ge rich glasses, the main building blocks are the ethane-like structures containing Ge-Ge bonds, which can be easily destroyed as such. This process is facilitated by the lower bond energy of the Ge-Ge bonds – 263 kJ/mol. The defects created in this manner react with oxygen, forming Ge-O bonds. This mechanism shows the importance of availability of Ge atoms for oxidation to occur. It is for this reason that the photo-oxidation happens more easily in Ge rich glasses than in the Se rich compositions.

During the oxidation, a part of Ge, which otherwise would form structural units with S, reacts with oxygen and is taken out from the initial chalcogenide backbone. Since the number of S atoms remains unchanged, the ratio between them and the remaining Ge atoms within the Ge-chalcogen network increases, so that the Raman spectrum exhibits structural characteristics of S-rich glasses. We, however, miss a clear signal from the oxidized part of Ge since it is much weaker than the one from the Ge-chalcogen bonds. This description of oxidation induced changes is clearly demonstrated in figure 3 where the dominance of the peak at 340 cm^{-1} develops with the time of illumination. It is attributed mainly to the breathing

mode of the corner-sharing tetrahedral units [23]. These results indicate significant reorganization of the structure of the films caused by illumination and subsequent oxidation after 20 minutes of illumination in air. As mentioned above, we could not prove by Raman spectroscopy the presence of GeO_2 which has breathing modes of lower intensity at 400 cm^{-1} [24], or the broad tail extending to 650 cm^{-1}[25]. There are fringes in the colored area on figure 6. They must be Newton rings, caused by the presence of thin layers with different refractive index values. For that reason, we assume that there is a layer composed of germanium dioxide (GeO_2) completely transparent for visible light on the surface, and a Ge-S film with a different color is positioned below this layer. This assumption explains why some authors report a decrease in film thickness based on optical measurements.

One aspect that has not been addressed sufficiently is how oxidation affects the photodiffusion of Ag in ChG. In this regard, we note that the photodiffusion products are different in the presence of oxygen. In a previous study of photo-oxidation of Ge-S glasses [26], we found that the oxidation process is not limited only to the surface, but once started it progresses deeper into the film. Since the GeO_2 layer is transparent to the blue light, used in the cited study, the laser affects the Ge-S bonds at the interface between GeO_2 layer and Ge-S layer and produces dangling Ge atoms in the heterogeneous structure. In order to achieve the progression of the oxidation front, re-organization of the Ge-O network is required with the supply of oxygen from the exposed surface, so that Ge becomes consumed in the oxidation process and the Ge/S ratio available for the establishment of the Ge-S network diminishes. As demonstrated in figure 3, the reformed network has the structural characteristics of glasses enriched in S. We suggest that this variety of structural building blocks that form after oxidation is the main reason for the observation of three different types of diffusion products containing Ag in the XRD pattern: α– and β–Ag_2Se and Ag_8GeSe_3 (figure 10).

We believe that the absence of oxygen lowers chemical potential that drives Ag into the Ge-Se network due to the limited number of charged defects forming in the system due to illumination with light. In this case the $Ge_{30}Se_{70}$ network is built up by standard tetrahedral structure, fully consuming the available Se atoms so that the diffused Ag ions are restricted to bonding with some defects existing on these structural units. It is for this reason that the XPS data reveal formation of uniform structure with ethane-like fragments only and Ag^+ ions between them. By comparison, when oxygen is present, Ag reacts with the high number of charged defects occurring at illumination, forming a variety of diffusion products, as revealed by the XRD results (figure 10). The reason for this variety is the fact that the chalcogens upon oxidation are in multiple environments due to extraction of some Ge atoms from the Ge-Se network. Then the chalcogen atoms form binary structures with Ag, which is not the case in absence of oxygen. This distinction is in a good agreement with the fact that, the binding energies of Ag $3d_{5/2}$ core level peaks significantly differs (~1 eV) when the photodiffusion of silver occurs in the presence vs. absence of oxygen. In the presence of oxygen silver is a part of the matrix forming mostly covalent bonds. In the absence of oxygen the position of the Ag $3d_{5/2}$ core level peak corresponds to Ag^+ ions connected with glassy matrix [16].

5. Conclusions

We have established that in Ge-chalcogenide systems photo-oxidation is manifested essentially as a reaction of oxygen with Ge. This reaction is very much structure sensitive and occurs much more easily when the weaker Ge-Ge bonds are available in the ChG network. The oxidation process is not limited only to the surface since as the reaction progresses, structural reorganization occurs which facilitates supply of oxygen to the interface between the oxidized phase and the remaining chalcogenide network. In contrast to photodiffusion of silver in vacuum, where Ag is present in an ion form, the products of photodiffusion in an oxygen containing environment are a mixture of binary and ternary Ag compounds.

Acknowledgements

The authors thank to Phoseon Technology for providing the UV LED system. The work was partially supported by U.S. National Science Foundation, through International Materials Institute for New Functionality in Glass, IMI-NFG (NSF Grant No. DMR-0409588 and DMR-0844014).

References

[1] M. N. Kozicki, S. W. Hsia, A. E. Owen, P. J. S. Ewen, J. Non-Cryst. Sol. **137&138** 1341 (1991).
[2] N. Yoshida, M. Itoh, K. Tanaka, J. Non-Cryst. Sol. **198-200**, 749 (1996).
[3] K. Shimakawa, A. V. Kolobov, S. R. Elliot, Adv. in Phys. **44**, 475 (1995).
[4] A. Ganjoo, K. Shimakawa, K. Kitano, E. A. Davis, J. Non-Cryst. Sol. **299-302,** 917 (2002).
[5] G. Chen, H. Jain, M. Vlcek, S. Khalid, J. Li, D. A. Drabold, S.R. Elliott, Appl. Phys. Lett. **82,** 706 (2003).
[6] H. Fritzsche, in Insulating and Semiconducting Glasses, P. Boolchand editor, World Scientific, Singapore, New Jersey, London, Hong Kong, 2000 p. 653.
[7] S. Rajagopalan, K. S. Harshawardhan, L. K. Malhotra, K. L. Chopra, J. Non-Cryst. Sol. **50**, 29 (1982).
[8] K. Tanaka, Y. Kasanuki A. Odjima, Thin Solid Films **117** 251 (1984).
[9] C. A. Spence, S. R. Elliott, Phys. Rev. B**39**, 5452 (1989).
[10] L. Tichy A. Triska, H. Ticha, N. Frumar, Phil. Mag. B **54**, 219 (1986).
[11] L. Tichy, H. Ticha, K. Handlir, J. Non-Cryst. Sol. **97-**

98, 1227 (1987).
[12] K.S. Harshavardhan, M. S. Hegde, Phys. Rev. Lett. **58** 567 (1987).
[13] T. Kawaguchi, S. Maruno, Ke. Tanaka, J. Appl. Phys. **73,** 4560 (1993).
[14] Y. Utsugi, M. Kakuchi, Rev. Sci. Instrum. **60** 2295 (1989).
[15] K.D. Kolwicz, M.S. Chang, J. Electrochem. Soc. **127** 135 (1980).
[16] A. Kovalskiy, A. C. Miller, H. Jain, M. Mitkova, J. Am. Ceram. Soc. **91**, 760 (2008).
[17] R. Golovchak, A. Kovalskiy, A.C. Miller, H. Jain, O. Shpotyuk, Phys. Rev. **B 76** 125208 (2007).
[18] M. Mitkova, M. N. Kozicki, H. C. Kim, T. L. Alford, *J. Non-Cryst. Sol.,* **338 & 340**, 552 (2004).
[19] S. Mamedov, D.G. Georgiev, Tao Qu, P. Boolchand, J. Phys.: Condens. Mat. **15** S2397 (2003).
[20] H. Takebe, H. Maeda and K. Morinaga, J. Non-Cryst. Solids **291**, 14 (2001).
[21] I. P. Kotsalas, and C. Raptis, Phys. Rev. **B 64**, 125210-1 (2001).
[22] CRC Handbook of chemistry and Physics, D.R. Lide Editor-in-Chief, 81st edition (2001)
[23] X. Feng, W.J. Bresser and P. Boolchand, Phys. Rev. Lett. **78,** 4422 (1997).
[24] Y. Kim, J. Saienga, S. W. Martin, J. Non-Cryst. Sol. **351,** 1973 (2005).
[25] M. Yamaguchi, T. Shibata, and Ke. Tanaka, J. Non-Cryst. Solids **232-234**, 715 (1998).
[26] Y. Sakaguchi, D. Tenne, M. Mitkova, phys. stat. sol. B **246**(8), 1813 (2009)

*Corresponding author: mariamitkova@boisestate.edu